frontiers | Frontiers in Marine Science

TYPE Original Research
PUBLISHED 01 September 2025
DOI 10.3389/fmars.2025.1600122

OPEN ACCESS

EDITED BY
Martin F. Soto-Jimenez,
National Autonomous University of Mexico, Mexico

REVIEWED BY
Yoshihisa Mino,
Nagoya University, Japan
Sergio Aguíñiga-García,
National Polytechnic Institute (IPN), Mexico

*CORRESPONDENCE
Xingchen Tony Wang
xingchen.wang@bc.edu

†These authors have contributed equally to this work and share first authorship

‡Deceased

RECEIVED 25 March 2025
ACCEPTED 17 July 2025
PUBLISHED 01 September 2025

CITATION
Kong T, Lee T, Landry K, Zhai R, Dong S and Wang XT (2025) Evaluating foraminifera-bound $\delta^{15}N$ as an ocean deoxygenation proxy: the influence of oxygen-deficient zone depths. *Front. Mar. Sci.* 12:1600122. doi: 10.3389/fmars.2025.1600122

Evaluating foraminifera-bound $\delta^{15}N$ as an ocean deoxygenation proxy: the influence of oxygen-deficient zone depths

Tianshu Kong[1†], Thomas Lee[1†], Kameko Landry[1†], Ruixiang Zhai[1], Sijia Dong[2‡] and Xingchen Tony Wang[1*]

[1]Department of Earth and Environmental Sciences, Boston College, Chestnut Hill, MA, United States, [2]School of Sustainable Energy and Resources, Nanjing University, Nanjing, China

The nitrogen isotopic composition of shell-bound organic matter in planktonic foraminifera (FB-$\delta^{15}N$) is widely used as a proxy for past ocean deoxygenation because water-column denitrification in oxygen-deficient zones (ODZs; $[O_2] < 5$ μmol/kg) preferentially removes ^{14}N, enriching the remaining nitrate in ^{15}N. Typically, increases in FB-$\delta^{15}N$ records from ODZ-influenced regions are interpreted as evidence of ODZ expansion or intensification. However, planktonic foraminifera predominantly feed on organic nitrogen derived from the subsurface nitrate immediately below the euphotic zone, often above ODZ core depths. It remains unclear if the $\delta^{15}N$ maxima observed within ODZ cores, reflecting denitrification intensity at a given location, directly correlates with the FB-$\delta^{15}N$ values recorded above. Here, we combine new and published data from the eastern tropical Pacific ODZs to examine relationships among subsurface nitrate $\delta^{15}N$, ODZ $\delta^{15}N$ maxima, and ODZ upper-boundary depths. Our analysis reveals a strong correlation between subsurface nitrate $\delta^{15}N$ and ODZ $\delta^{15}N$ maxima (R^2 = 0.56-0.79), supporting the use of FB-$\delta^{15}N$ as an indicator of denitrification intensity within ODZ regions. However, subsurface nitrate $\delta^{15}N$ also correlates strongly with the ODZ upper-boundary depth (R^2 = 0.57-0.59), with lower $\delta^{15}N$ values observed where ODZs are deeper. For example, at our new study sites in the Eastern Tropical North Pacific (5 – 8°N), where the ODZ upper-boundary depth is ~300 m, the $\delta^{15}N$ maxima (>10‰) at the ODZ core decrease upward to subsurface nitrate $\delta^{15}N$ values of ~6.5‰ — only slightly higher than the global pycnocline nitrate $\delta^{15}N$. These results suggest that variations in ODZ depth should be accounted for when interpreting FB-$\delta^{15}N$ records (and other $\delta^{15}N$ archives) from ODZ regions. Under warmer conditions, organic matter remineralization may become shallower due to the temperature dependence of respiration, shifting ODZs upward and elevating FB-$\delta^{15}N$ even without changes in denitrification rates. To more robustly reconstruct ODZ history using FB-$\delta^{15}N$, we recommend using multiple sites from the ODZ interior to regions beyond their modern boundaries. Cores situated outside

modern ODZs, where thermocline nitrate $\delta^{15}N$ still carries the ODZ signature, are ideal for tracing ODZ expansions and contractions, while cores from within the modern ODZs provide complementary constraints on ODZ intensity and vertical structure.

KEYWORDS

planktonic foraminifera, nitrogen isotopes, ocean deoxygenation, marine nitrogen cycle, paleoceanography

1 Introduction

The nitrogen isotopic composition of shell-bound organic matter in planktonic foraminifera (foraminifera-bound $\delta^{15}N$, or FB-$\delta^{15}N$, where $\delta^{15}N = \{[(^{15}N/^{14}N)_{sample}/(^{15}N/^{14}N)\ N_{2\ in\ air}] - 1\} \times 1000‰$) has emerged as a powerful proxy for reconstructing past changes in the marine nitrogen cycle and its interaction with climate (*e.g.*, Ren et al., 2009; Kast et al., 2019; Studer et al., 2021; Auderset et al., 2022; Wang et al., 2022). In regions with complete surface nitrate consumption such as oligotrophic gyres, FB-$\delta^{15}N$ are correlated with the $\delta^{15}N$ of the subsurface nitrate (*i.e.*, immediately below the euphotic zone) (Ren et al., 2009, 2012; Schiebel et al., 2018; Smart et al., 2018; Robinson et al., 2023). In regions with incomplete nitrate consumption such as the Southern Ocean, FB-$\delta^{15}N$ is also indicative of the degree of nitrate consumption in the past (Martínez-García et al., 2014). Compared with other $\delta^{15}N$ archives, FB-$\delta^{15}N$ offers several advantages. First, relative to bulk sedimentary $\delta^{15}N$ records, FB-$\delta^{15}N$ is less affected by diagenesis because the shell-bound organic matter is protected by the calcite shells (Ren et al., 2009). Second, foraminifera are more widely distributed throughout the ocean than other fossil-bound $\delta^{15}N$ archives such as diatoms and corals. Third, foraminifera can be readily separated from ocean sediments via sieving and picking, enabling species-specific $\delta^{15}N$ analyses that mitigate complications arising from shifts in species composition. Fourth, each FB-$\delta^{15}N$ measurement integrates 500-1,000 individuals, providing a statistically robust average $\delta^{15}N$ value over hundreds of years. Collectively, these characteristics make FB-$\delta^{15}N$ an ideal proxy for systematically reconstructing historical changes in the marine nitrogen cycle.

One notable application of the FB-$\delta^{15}N$ proxy is in reconstructing ocean deoxygenation in the eastern tropical Pacific, which hosts the world's largest oxygen-deficient zones (ODZs; typically defined as < 5 μmol/kg O_2). In this region, upwelling brings nutrient-rich waters to the surface and boosts productivity (Chavez and Barber, 1987; Fiedler et al., 1991), while sluggish thermocline circulation leads to poor ventilation and limited oxygen replenishment (Luyten et al., 1983). This combination leads to the development of the largest ODZs in the ocean (Fiedler and Talley, 2006; Paulmier and Ruiz-Pino, 2009). These ODZs affect human societies by reducing marine biodiversity, disrupting food webs, and adversely affecting fish stocks (Breitburg et al., 2018). Moreover, the low oxygen environment promotes water column denitrification, thereby increasing the losses of fixed nitrogen from the ocean (Gruber, 2008; DeVries et al., 2012). During denitrification, the lighter isotope ^{14}N is preferentially removed, leading to higher $\delta^{15}N$ in the residual nitrate in the thermocline water (Cline and Kaplan, 1975; Liu and Kaplan, 1989). This high-$\delta^{15}N$ thermocline nitrate is subsequently transported to the euphotic zone above or adjacent to the ODZs, thereby elevating the $\delta^{15}N$ in both the upper ocean ecosystem and in FB-$\delta^{15}N$. Consequently, an increase in FB-$\delta^{15}N$ in regions influenced by ODZs is interpreted as indicative of ODZ expansion or intensification.

To predict how ODZs might respond to anthropogenic climate change, studies have used FB-$\delta^{15}N$ to reconstruct past variations in the extent and intensity of ODZs, spanning timescales from the early Cenozoic to the Holocene (Kast et al., 2019; Studer et al., 2021; Auderset et al., 2022; Wang et al., 2022; Hess et al., 2023; Moretti et al., 2024; Yao et al., 2024). For example, lower $\delta^{15}N$ values observed during the warm mid-Miocene were used to suggest that the eastern Pacific ODZs were smaller than they are today, contrary to some climate model predictions (Auderset et al., 2022; Hess et al., 2023). Despite these valuable applications, important questions remain regarding the calibration of FB-$\delta^{15}N$ proxy in modern eastern tropical Pacific ODZs. Although it is generally assumed that FB-$\delta^{15}N$ records from regions influenced by ODZs reflect the intensity and extent of ODZs, the depth of the $\delta^{15}N$ maxima at the core of ODZs, which reflects relative denitrification intensity at a given station, is often deeper than the depth of subsurface nitrate $\delta^{15}N$ recorded by planktonic foraminifera. Thus, the upward transfer of the ODZ $\delta^{15}N$ signal to the subsurface may be further complicated by factors such as the depth of ODZs.

In this study, we aim to further validate FB-$\delta^{15}N$ as an ocean deoxygenation proxy in the eastern tropical Pacific. We report new sediment core-top FB-$\delta^{15}N$ measurements from three to five foraminifera species with corresponding water-column nitrate $\delta^{15}N$ from samples collected at three stations during the R/V Sally Ride cruise SR2113 in November to December 2021 in the Eastern Tropical North Pacific (ETNP) region (4.8°N-6.0°N, 86.6° W-88.0°W). Combining these data with published $\delta^{15}N$ data from the eastern tropical Pacific ODZs, we examine the relationship

among subsurface nitrate $\delta^{15}N$ (thus FB-$\delta^{15}N$), ODZ $\delta^{15}N$ maxima, and the depth of the ODZ upper boundary. In addition, we investigate differences in $\delta^{15}N$ between symbiont-bearing, surface-dwelling species and symbiont-barren, deep-dwelling species, and examine how hypoxic conditions above ODZs influence foraminiferal assemblages and abundance, as well as inter-species $\delta^{15}N$ differences.

2 Materials and methods

2.1 Compilation and analysis of published nitrate $\delta^{15}N$ from eastern tropical Pacific ODZs

We have compiled and analyzed published nitrate $\delta^{15}N$ and concentration data from the eastern tropical Pacific ODZs (Figures 1c, d; 2, Supplementary Figures S1, S2; Supplementary Data) (Brandes et al., 1998; Voss et al., 2001; Sigman et al., 2005; Rafter et al., 2012; Casciotti et al., 2013; Rafter and Sigman, 2016; Peters et al., 2018a, 2018b; Fripiat et al., 2021; Lee et al., 2025). Detailed information on station locations, water depths, nitrate $\delta^{15}N$ values, and nitrate concentrations is provided in the Supplementary Data. Oxygen concentration values (Supplementary Figure S1) were directly obtained from the respective studies. Specifically; all oxygen concentration data for the Eastern Tropical South Pacific (ETSP) are available in these original sources, whereas only 18 out of 26 stations in the ETNP include oxygen concentration data (Voss et al., 2001; Sigman et al., 2005; Lee et al., 2025).

In our analysis, subsurface nitrate $\delta^{15}N$ is defined as the average $\delta^{15}N$ between 150 m and 200 m at each station. If a station lacks data within this depth range, we linearly interpolate the nitrate $\delta^{15}N$ values at 150 m and 200 m based on the nearest available depth measurements and compute their average. The ODZ nitrate $\delta^{15}N$ maxima is defined as the highest nitrate $\delta^{15}N$ observed within the ODZs (O_2 < 5 µmol/kg). To determine the ODZ upper-boundary depth, we applied linear interpolation to detailed oxygen concentration profiles (Supplementary Data) and calculate the depth where the oxygen concentration falls below 5 µmol/kg. When these profiles were unavailable, we estimated the ODZ upper-boundary depth using data from the Kwiecinski and Babbin (Figure 1a; Kwiecinski and Babbin, 2021)

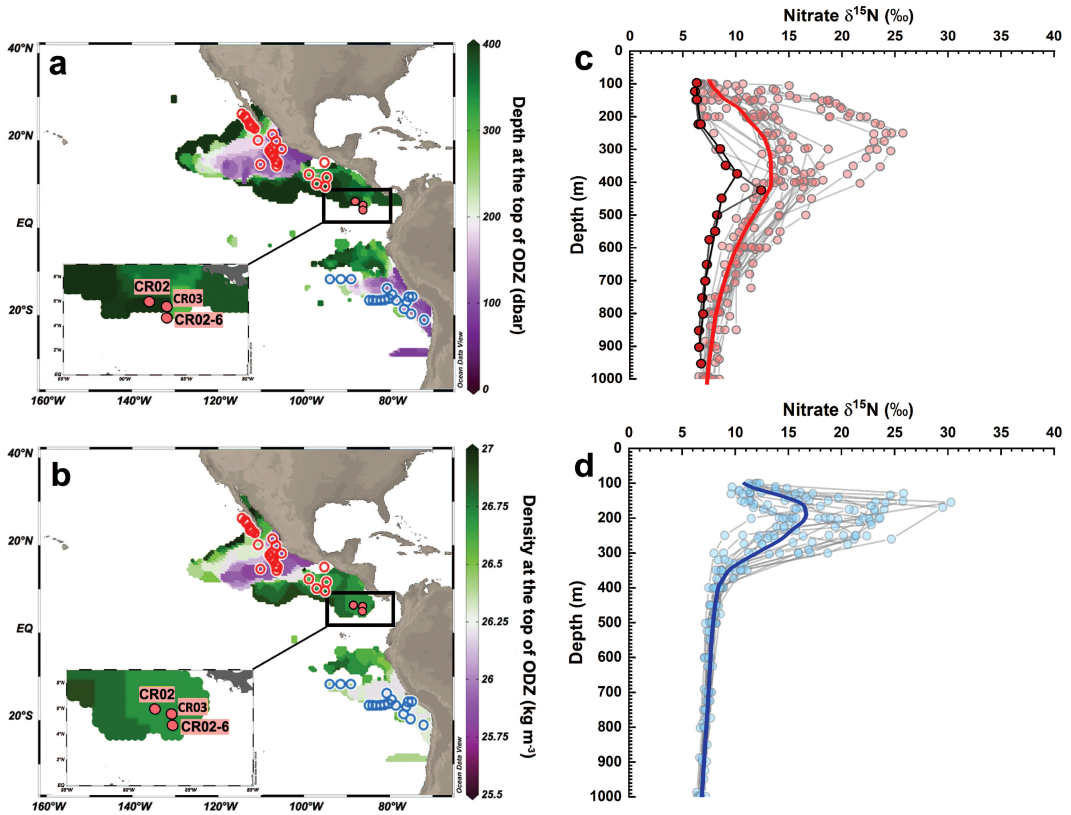

FIGURE 1
Compilation of new and published nitrate $\delta^{15}N$ data from the eastern tropical Pacific ODZs. Maps on the left display the upper boundary of the ODZs is as **(a)** depth (dbar) and **(b)** potential density (kg m^{-3}) (Data obtained from (Kwiecinski and Babbin, 2021)). Circles indicate nitrate $\delta^{15}N$ sampling locations in the Eastern Tropical North Pacific (ETNP, red circle, n=26) and the Eastern Tropical South Pacific (ETSP, blue circle, n=18). Empty circles represent stations from previous studies, while solid circles indicate the stations from this study. Nitrate $\delta^{15}N$ depth profiles are shown for each station in **(c)** the ETNP (including data from this study) and **(d)** the ETSP. Red circles outlined in black in **(c)** correspond to stations [maps **(a, b)**] from this study. Thick red and dark blue lines in **(c)** and **(d)** represent averaged $\delta^{15}N$ profiles for the ETNP and ETSP, respectively, calculated from both previous and current study stations. Maps were generated using Ocean Data View.

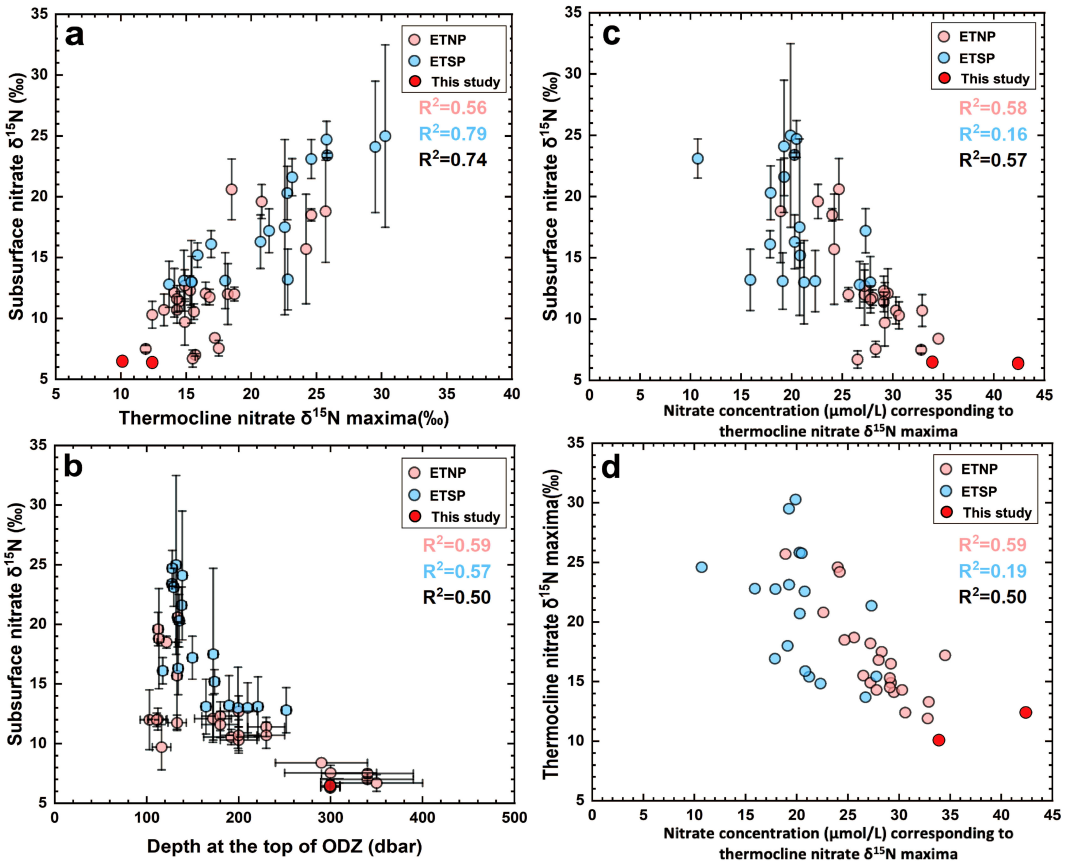

FIGURE 2
Relationship among subsurface $\delta^{15}N$, thermocline $\delta^{15}N$ maxima, and ODZ depths in the eastern tropical Pacific ODZs. **(a)** Comparison of subsurface $\delta^{15}N$ with thermocline $\delta^{15}N$ maxima at the same stations. **(b)** Comparison of subsurface $\delta^{15}N$ with depth at the ODZ upper boundary. **(c)** Comparison of subsurface $\delta^{15}N$ with thermocline nitrate concentration at the depth of ODZ $\delta^{15}N$ maxima. **(d)** Comparison of thermocline $\delta^{15}N$ maxima with thermocline nitrate concentration at corresponding depths. Dark red dots represent data from this study; light red dots represent data from previous ETNP studies; and blue dots indicate previous ETSP studies. R^2 values are annotated in each plot: red corresponds to ETNP (previous and current data), blue to ETSP, and black to the combined dataset of both ETNP and ETSP. Most p-values across our regression analyses are statistically significant ($p < 0.05$), except for the ETSP cases in **(c)** ($p = 0.1$) and **(d)** ($p = 0.07$).

in combination with the nitrate $\delta^{15}N$ depth profiles (Figures 1c, d; Supplementary Data). Error bars (1sd) were calculated based on the standard deviation of the two datasets. We excluded stations in which the ODZ upper-boundary depth is shallower than 100 m, because in such cases the contributions of denitrification and nitrate assimilation to subsurface nitrate $\delta^{15}N$ cannot be reliably separated.

To illustrate the differences between the ETNP and ETSP, averaged depth profile of nitrate $\delta^{15}N$ in both ODZ regions, were generated using Python by sampling y-values at 100 evenly spaced points along the full x-range, stacking the values into arrays, and computing the mean at each position.

2.2 Statistical methods for assessing controls on subsurface nitrate $\delta^{15}N$

To evaluate the independent and combined influences of thermocline nitrate $\delta^{15}N$ maxima and the ODZ upper-boundary depth on subsurface nitrate $\delta^{15}N$, we employed multiple statistical approaches, including multiple linear regression, Pearson correlation analysis, and multicollinearity diagnostics using Variance Inflation Factors (VIFs).

We developed multiple linear regression models separately for the ETNP, ETSP, and the combined dataset. These models allowed us to quantify the individual and joint contributions of thermocline $\delta^{15}N$ maxima and ODZ upper-boundary to variations in subsurface nitrate $\delta^{15}N$. The general form of the regression model is (Jobson, 1991):

$$Subsurface\ \ nitrate\ \ \delta^{15}N = \beta_0 + \beta_1(thermocline\ \ nitrate\ \ \delta^{15}N\ \ maxima) + \beta_2(ODZ\ \ upper\text{-}boundary\ \ depth)$$

Pearson correlation coefficients (r) were calculated to quantify linear relationships among the variables: subsurface nitrate $\delta^{15}N$, thermocline nitrate $\delta^{15}N$ maxima, and ODZ upper-boundary depth. The Pearson correlation coefficient is defined as follows (Kutner, 2005):

$$r = \frac{\sum_{i=1}^{n}(x_i - \bar{x})(y_i - \bar{y})}{\sqrt{\sum_{i=1}^{n}(x_i - \bar{x})^2}\sqrt{\sum_{i=1}^{n}(y_i - \bar{y})^2}}$$

where x_i and y_i represent paired observations, $\bar{x}$ and $\bar{y}$ denote their respective means.

To assess multicollinearity between predictor variables, we computed the Variance Inflation Factor (VIF). The VIF quantifies the extent to which collinearity among predictors inflates the variance of estimated regression coefficient and is calculated as follows (Kutner, 2005),

$$VIF = \frac{1}{1 - r^2}$$

where r is the Pearson correlation between the predictor variables. A high VIF value indicates significant multicollinearity, suggesting caution when interpreting regression results.

2.3 Sample collection

Sediment core-top and water column samples were collected from three stations (Figures 1a, b) during the R/V Sally Ride SR2113 expedition spanning in November-December 2021 in the ETNP. These stations included CR02 (longitude: 88.0° W, latitude: 6.0° N, depth:2640.0m), CR03 (longitude: 86.6° W, latitude: 5.4° N, depth:1774.4m), and CR02-6 (longitude: 86.6° W, latitude: 4.8° N, depth: 1268.1m).

Sediment samples were collected via Multi Cores at the stations, using an Ocean Instruments MC-800 multi-corer with polycarbonate liners (i.d. = 9.6 cm). Cores were immediately extruded and sectioned upon recovery, and discrete sediment samples were stored in a 0°C walk-in freezer on board the ship before transport back to shore. Once in the lab, bulk sediment samples were dried in an oven at 50°C for 72 hours. The core lengths for CR02, CR03, and CR02–6 were 36 cm, 22 cm, and 28 cm, respectively. The sediment core-tops (0–10 cm) were sectioned into 1 cm intervals. After drying, portions of the sediment were left unground for various analyses, while the remainder was preserved for further lab analyses.

For foraminifera separation, the core-top sediment samples were transferred into 500 ml conical flasks, soaked in Milli-Q water, and then placed on an orbital shaker overnight. Following this step, the mixture was wet sieved through a 250 μm mesh. Gentle manual agitation was used to remove adherent sediment from the foraminifera. The separated foraminifera samples were collected from the sieve, transferred into 15 ml polypropylene centrifuge tubes (BD Falcon), and dried at 55°C for 7 days.

2.4 Foraminifera identification, counts, and picking

Five species of planktonic foraminifera (section 3.2) were identified in sufficient quantities, allowing for the collection of at least 3 mg per species. The morphology of these species was determined following the classifications of d'Orbigny (1839) and Brady (1877). The equation for determining relative abundance of each species is from Achacoso et al. (2016):

$$Relative\ \ Abundance\ \ (\%) = \frac{The\ \ number\ \ of\ \ individuals\ \ of\ \ the\ \ same\ \ species}{Total\ \ number\ \ of\ \ individuals\ \ for\ \ all\ \ species} \times 100$$

The sorted foraminifera were carefully transferred from the centrifuge tubes to a sectioned tray for examination under a VWR laboratory led zoom stereo binocular microscope. Using brushes of varying sizes, individual foraminifera specimens were picked and placed onto 4-hole hard paper slides. A cover glass slide and a removable metal brace were then applied to securely protect each slide. To ensure an exhaustive collection, each sample was reviewed multiple times, guaranteeing the selection of at least 3 mg of the specified foraminifera species and thorough examination of the entire sample before proceeding to the next set.

2.5 FB-δ^{15}N analyses

The picked foraminifera samples were gently crushed to open their chambers using a glass rod and transferred to 15ml centrifuge tubes. Impurities were removed by treating each sample with 10 ml of 2% sodium polyphosphate and sonicating for 2–5 minutes. The solution was then decanted, and the foraminifera were rinsed three times with Milli-Q water. Next, 10 ml of the dithionite-citric acid mixture (pH ~8) was added to each vial (Mehra and Jackson, 1958). The vials were placed in an 80°C water bath for an hour and were shaken once during the period. After that, the dithionite-citric acid solution was decanted and the foraminifera were rinsed three times with Milli-Q water again.

After the reductive cleaning step, ~10 ml of sodium hypochlorite (10-15% available chlorine) was added to each sample, which is then placed on an orbital-shaker overnight (>12 hours). After that, the sodium hypochlorite solution was decanted and rinsed three times with Milli-Q water. The samples were then carefully transferred into 4 ml pre-combusted glass vials, and all remaining Milli-Q water was removed with a vacuum pump. The samples were then dried in an oven at 55°C overnight. In each batch of analyses, three replicates of a coral standard (CBS-II) were included following the same cleaning procedures, serving as quality control of the cleaning protocol.

After drying, the cleaned foraminifera samples were weighed and transferred into another 4 ml pre-combusted glass vial. Then, 3–7 mg of foraminifera were dissolved in 50 μl 4 N HCl to release the shell-bound organic N into solution. The released organic nitrogen was then oxidized into nitrate by adding 1 ml of the persulfate oxidizing reagent (POR), prepared by dissolving 1g of low-N recrystallized persulfate and 2 g NaOH in 100 ml of distilled, low-N Milli-Q water. In this step, amino acid standards (USGS 64 and 4 USGS 65) and POR blanks were included to account for the contribution of blanks during the oxidation processes. The samples were autoclaved for 1 hour to ensure complete oxidation, then

centrifuged at 4000 rpm for 10 minutes. After transferring the supernatant to a new vial, the pH of each sample was adjusted to neutral with 4 N HCl and 2 N NaOH.

After the oxidation step, the resulting nitrate was converted to nitrous oxide using the 'denitrifier method' using *Pseudomonas chlororaphis* that lacks nitrous oxide reductase (Sigman et al., 2001; Weigand et al., 2016). The $\delta^{15}N$ of the resulting N_2O in the headspace of the vials was then measured on a customized Gas Bench coupled to a Thermo-Fischer Scientific Delta V isotope ratio mass spectrometer. Nitrate isotope standards IAEA-N3 and USGS-34 were analyzed along with the samples, which are used for calibrating the reported $\delta^{15}N$ values (‰ vs. air). The final FB-$\delta^{15}N$ precision, based on replicate analyses, is 0.2‰.

2.6 Water column nitrate $\delta^{15}N$

Water nitrate $\delta^{15}N$ samples were collected through Conductivity, Temperature, Depth (CTD) casts using the 10-L Niskin Rosette at 4 stations. Samples were collected from approximately 24 depths ranging from 7–2900 m. The shallowest samples were collected first to avoid nitrate contamination from higher nitrate waters deeper in the water column. Samples were filtered through a 0.2 µm PVDF luerlock filter attached to a syringe. Once filtered, samples were stores in 30 ml pre-acid-washed HDPE bottles and immediately frozen until analysis. Nitrate $\delta^{15}N$ (Landry and Wang, 2024) in these samples were then measured using the "denitrifier method" described in section 2.3 with *Pseudomonas aureofaciens* (Weigand et al., 2016).

3 Results

3.1 Relationship among subsurface nitrate $\delta^{15}N$, ODZ nitrate $\delta^{15}N$ maxima, and ODZ depths in the eastern tropical Pacific ODZs

The ETNP and ETSP host two of the largest ODZs in the global ocean. The ETNP ODZ is deeper and more expansive, with the average ODZ upper-boundary depth around 279 dbar (or meters), extending beyond 800 dbar in core regions (Kwiecinski and Babbin, 2021). In comparison, the ETSP ODZ starts at a shallower average depth of approximately 246 dbar and has an average thickness of 108 dbar (Kwiecinski and Babbin, 2021). In terms of scale, the ETNP ODZ ($[O_2] < 5$ µmol/kg) encompasses a significantly larger volume, estimated at 0.6-2.4 × 10^6 km^3 (Bianchi et al., 2012) and covers a horizontal area of up to 4.27 × 10^6 km^2 (Kwiecinski and Babbin, 2021). The ETSP ODZ is smaller, with a volume of about 0.4-6.1 × 10^5 km^3 (Bianchi et al., 2012) and a surface extent of 2.3 × 10^6 km^2 (Kwiecinski and Babbin, 2021). Both the ETNP and ETSP ODZs are associated with similar potential densities, averaging approximately 26.5 kg/m^3 (Kwiecinski and Babbin, 2021). The larger size and stability of the ETNP ODZ results from weaker ventilation, which leads to persistently low oxygen concentrations (Supplementary Figure S1) with less variability throughout the upper 1000 m of the water column (Supplementary Figure S2). In contrast, the ETSP ODZ is influenced by the Peru–Chile Undercurrent (PCUC) and stronger eddy-driven mixing, which periodically introduce oxygenated water, making it thinner and less stable than the ETNP ODZ (Czeschel et al., 2015; Margolskee et al., 2019).

Mean subsurface nitrate $\delta^{15}N$ values in the compiled dataset are higher in the ETSP (mean = 17.9‰) than in the ETNP (mean = 11.7‰). Similarly, thermocline nitrate $\delta^{15}N$ maxima are higher in the ETSP (mean = 21.1‰) than in the ETNP (mean = 16.5‰). A significant positive correlation between subsurface nitrate $\delta^{15}N$ and thermocline nitrate $\delta^{15}N$ maxima is observed (Figure 2a, ETNP: $R^2 = 0.56$, $p < 0.05$; ETSP: $R^2 = 0.79$, $p < 0.05$). In addition, a significant relationship between subsurface nitrate $\delta^{15}N$ and ODZ upper-boundary depth is observed (Figure 2b; ETNP: $R^2 = 0.59$, $p < 0.05$; ETSP: $R^2 = 0.57$, $p < 0.05$). Furthermore, the ETNP exhibits robust inverse correlation between subsurface nitrate $\delta^{15}N$ and thermocline nitrate concentrations at the depth of thermocline nitrate $\delta^{15}N$ maxima (Figure 2c, $R^2 = 0.58$, $p < 0.05$), as well as between thermocline nitrate $\delta^{15}N$ maxima and corresponding nitrate concentrations (Figure 2d, $R^2 = 0.59$, $p < 0.05$). In contrast, the ETSP shows weaker inverse relationships (Figure 2c, $R^2 = 0.16$, $p = 0.1$; and Figure 2d, $R^2 = 0.19$, $p = 0.07$). However, combining data from both regions yields consistently strong correlations.

Our statistical analyses indicate that both thermocline nitrate $\delta^{15}N$ maxima and ODZ upper-boundary depth independently and significantly influence subsurface nitrate $\delta^{15}N$ across the ETNP, ETSP, and combined datasets. In the ETNP, the best-fit linear model explains 73% of the variance in subsurface $\delta^{15}N$ (Table 1, $R^2 = 0.73$, $p < 0.001$). In the ETSP, the best-fit linear model explains 83% of the variance (Table 1, $R^2 = 0.83$, $p < 0.001$). Combining ETNP and ETSP data, the best-fit linear model explains 80% of the variance (Table 1, $R^2 = 0.80$, $p < 0.001$).

Pearson correlations confirm strong positive relationships between subsurface nitrate $\delta^{15}N$ and thermocline nitrate $\delta^{15}N$ maxima ($r = 0.74$ to 0.89), and strongly negative correlations with ODZ depth ($r = -0.71$ to -0.77) (Table 2). The negative correlation between thermocline nitrate $\delta^{15}N$ maxima and ODZ depth is moderate ($r = -0.56$ to -0.70) (Table 2) suggesting that these two predictors are related but not strongly coupled. Consistent with these findings, all VIF values remained low (range: 1.46-1.97; Table 3), confirming minimal multicollinearity.

3.2 Foraminifera abundance

Three different foraminiferal groups were analyzed in this study: deeper-dwelling, non-symbiont bearing, non-spinose species (*G. tumida*); deeper-dwelling, symbiont bearing, non-spinose species (*N. dutertrei* and *G. menardii*); and surface dwelling, symbiont-bearing, spinose species (*G. sacculifer*, and *O. universa*). Their relative abundance varied across the stations

TABLE 1 Multiple linear regression coefficients (β_0, β_1, and β_2) and model performance (R^2 and F-statistic) are compared across the ETNP, ETSP, and the combined dataset.

	ETNP	ETSP	Combined
β_0 (Intercept)	8.75	9.27	5.28
β_1 (Thermocline nitrate $\delta^{15}N$ maxima)	0.48***	0.65***	0.72***
β_2 (ODZ depth)	-0.025***	-0.031***	-0.024***
R^2	0.73	0.83	0.80
F-statistic	31.54	35.62	82.57
Sample size	26	18	44

All coefficients showed statistically significant correlations ($p < 0.001$***) in both ETNP and ETSP regions. The regression model is: *Subsurface nitrate* $\delta^{15}N = \beta_0 + \beta_1$(*thermocline nitrate* $\delta^{15}N$ *maxima*) + β_2(*ODZ upper*-boundary depth)

(Supplementary Figure S3, Table 4). At stations CR02 and CR03, *N. dutertrei* and *G. menardii* dominated, each constituting approximately 45% of the total foraminiferal assemblage. *G. tumida* is the third most abundant species, accounting for 5-8%, with all other species collected accounted for less than 5%. At station CR02-6, N. *dutertrei* and *G. menardii* remained the most abundant (each ~30%). Of the other species present, *G. tumida* and *G. sacculifer* each contributed about 15-18%, while *O. universa* comprised roughly 5-8%.

3.3 Foraminifera-bound N isotopes

FB-$\delta^{15}N$ of individual species ranges from 5.2‰ to 9.2‰ (Figure 3b; Table 4). At station CR02, the FB-$\delta^{15}N$ values for three deep-dwelling species, *N. dutertrei*, *G. menardii*, and *G. tumida*, are 8.6‰, 8.6‰, and 8.7‰, respectively. At station CR03, these three species show an increase of approximately 0.5‰ compared to their counterparts at CR02, with values of 9.2‰, 9.2‰, and 9.2‰ respectively. At station CR02-6, these three deep-dwelling species exhibit values that are about 0.3‰ lower than those at CR03, recorded at 8.8‰, 8.9‰, and 9.0‰. Furthermore, the other two surface-dwelling species, *G. sacculifer* and *O. universa*, present values significantly lower than those of the deep-dwelling species, specifically, their values are 5.2‰ and 6.4‰.

TABLE 2 Pairwise pearson correlation coefficients (*r*) among subsurface $\delta^{15}N$, thermocline $\delta^{15}N$ maxima, and ODZ depth across the ETNP, ETSP, and combined dataset.

Relationship	ETNP	ETSP	Combined
Subsurface $\delta^{15}N$ and Thermocline nitrate $\delta^{15}N$ maxima	0.74	0.89	0.86
Subsurface $\delta^{15}N$ and ODZ depth	-0.77	-0.76	-0.71
Thermocline nitrate $\delta^{15}N$ maxima and ODZ depth	-0.56	-0.70	-0.59

Pearson correlation coefficients are interpreted as strong when $|r| \geq 0.7$, moderate when $|r|$ is between 0.4 and 0.7, and weak when $|r| < 0.4$ (Hinkle et al., 2003). All variable pairs show statistically significant correlations ($p < 0.001$) in both ETNP and ETSP regions.

TABLE 3 Variance Inflation Factors (VIFs) assessing multicollinearity between two predictors, thermocline $\delta^{15}N$ maxima and ODZ depth, across the ETNP, ETSP, and combined dataset.

Dataset	Pearson correlation (r)	r^2	VIF
ETNP	-0.56	0.31	1.46
ETSP	-0.70	0.49	1.97
Combined	-0.59	0.34	1.52

VIF values below 5 indicate low multicollinearity and suggest no concerns regarding multicollinearity (O'brien, 2007).

3.4 Water column profiles of nitrate $\delta^{15}N$ and dissolved oxygen concentration

In Figure 3b, the profiles for stations CR02 (green circles) and CR03 (yellow circles) exhibit similar trends, with nitrate $\delta^{15}N$ peaking at 12.4‰ and 10.1‰, respectively, around a depth of 400 m. Nitrate $\delta^{15}N$ values are 2–3‰ lower than the FB-$\delta^{15}N$ values of deep-dwelling species at corresponding depths (120–250 m, Farmer et al., 2007), which range from 6.2‰ to 6.8‰. The oxygen-deficient zone (dark grey box, with concentrations remaining below 5 µmol/kg) spans depths from 300 to 600 m. Additionally, oxygen concentrations drop below 63 µmol/kg between 70 and 1000 m, indicating the presence of a hypoxic zone (grey box).

4 Discussion

4.1 Influence of water-column denitrification and ODZ depths on FB-$\delta^{15}N$ as an ocean deoxygenation proxy

FB-$\delta^{15}N$ records are widely used to reconstruct past ocean deoxygenation (Kast et al., 2019; Auderset et al., 2022; Wang et al., 2022; Hess et al., 2023; Moretti et al., 2024) because of their sensitivity to water-column denitrification in ODZs. Typically, higher FB-$\delta^{15}N$ values are interpreted as reflecting an expansion of ODZs or intensification of denitrification. However, FB-$\delta^{15}N$ directly reflects the nitrate $\delta^{15}N$ in the subsurface, which is typically shallower than the core depths of the ODZs. The $\delta^{15}N$ maxima at the ODZ cores record the degree of water-column denitrification following Rayleigh fractionation (Sigman et al., 2005; Casciotti, 2016). Nitrate $\delta^{15}N$ decreases upward from the ODZ core to the subsurface due to mixing and other processes. It is unclear whether FB-$\delta^{15}N$ faithfully record the water-column denitrification occurring below. In our analysis of new and published nitrate $\delta^{15}N$ data from the eastern tropical Pacific ODZs, we demonstrate that subsurface nitrate $\delta^{15}N$ is well correlated with the ODZ $\delta^{15}N$ maxima (with an R^2 value of 0.56 to 0.79, $p < 0.05$). This high degree of correlation indicates that the water-column denitrification signal is effectively propagated to the subsurface nitrate $\delta^{15}N$ (thus FB-$\delta^{15}N$) above the ODZs, supporting the use of FB-$\delta^{15}N$ as a proxy for local water-column denitrification and ODZ intensity.

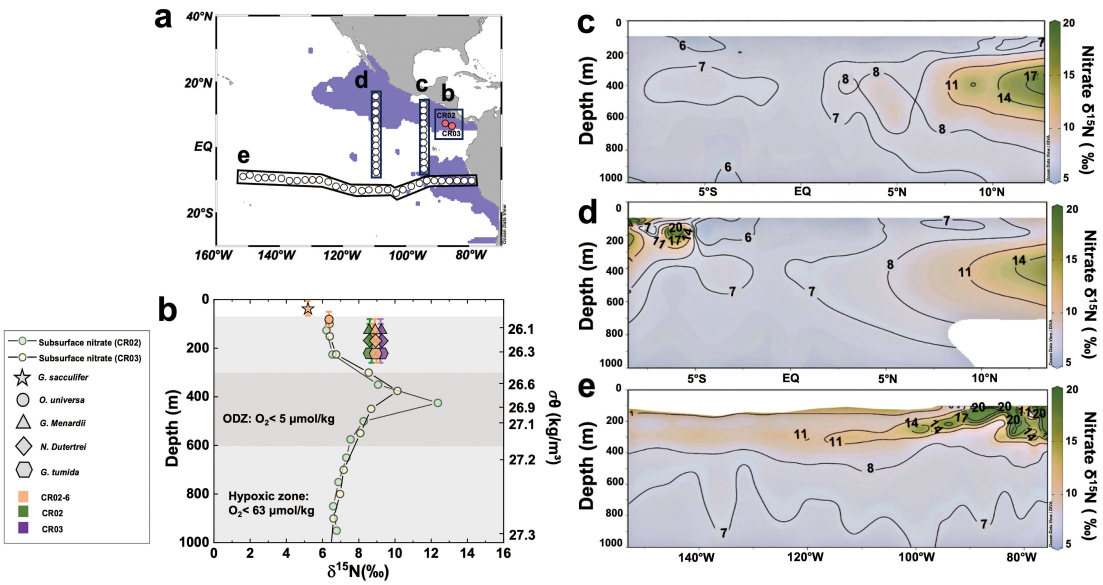

FIGURE 3
(a) Map of the eastern tropical Pacific oxygen deficient zone (ODZ, purple shading), showing locations of stations in this study (pink circles outlined in black, labeled b) and three nitrate $\delta^{15}N$ transects (white circles outlined in black, labeled c, d, and e). **(b)** Depth profile from the surface to 1000 m, displaying subsurface nitrate $\delta^{15}N$ (circles: green for station CR02, yellow for CR03) and dissolved oxygen concentration (shaded boxes: lighter grey indicating the hypoxic zone with [O2] < 63 µmol/kg, dark grey indicating the ODZ with [O2] < 5 µmol/kg). The potential density is shown on the right axis. Plotted alongside are FB-$\delta^{15}N$ from individual species at three stations (symbols). Global averaged habitat depth for each species, adapted from previous studies (Ravelo and Fairbanks, 1992; Farmer et al., 2007; Ren et al., 2009; Rebotim et al., 2017), are also shown: estimated habitat depths are *Globigerinoides sacculifer* (35 ± 30 m), *Orbulina universa* (75 ± 30 m), for *Globorotalia menardii* (110 ± 40 m), for *Neogloboquadrina dutertrei* (130 ± 40 m), and *Globorotalia tumida* (200 ± 50 m). **(c–e)** Published transects of nitrate $\delta^{15}N$ (depth:100m -1000m) in the eastern tropical Pacific to data from Rafter and Sigman (2016) and Peters (2018a). Maps (panels a, c-e) were generated using Ocean Data View.

TABLE 4 Planktonic foraminifera species, FB-$\delta^{15}N$ values, FB-$\delta^{15}N$ standard deviation, and relative foraminifera abundance in this study.

Station ID	Planktonic Foraminifera Species	FB-$\delta^{15}N$ (‰ vs. Air)	1SD based on sample replicates (‰ vs. Air)	Relative abundance (%)
CR02-6	*Globigerinoides sacculifer*	5.2	0.3	~15-18
	Orbulina universa	6.4	0.2	~5-8
	Globorotalia menardii	8.9	0.3	~30
	Neogloboquadrina dutertrei	8.8	0.03	~30
	Globorotalia tumida	9.2	0.2	~15-18
CR02	*Globorotalia menardii*	8.6	0.1	~45
	Neogloboquadrina dutertrei	8.6	0.2	~45
	Globorotalia tumida	8.7	0.2	~5-8
CR03	*Globorotalia menardii*	9.2	0.1	~45
	Neogloboquadrina dutertrei	9.2	0.1	~45
	Globorotalia tumida	9.2	0.2	~5-8

However, our analysis also reveals a complication of the FB-$\delta^{15}N$ deoxygenation proxy related to variations in ODZ depth. We find that subsurface nitrate $\delta^{15}N$ is correlated with the depth of the upper boundary of ODZs (with an R^2 value of 0.57 to 0.59, $p < 0.05$), with lower $\delta^{15}N$ values observed above deeper ODZs. In contrast, the Pearson Correlation Coefficients between thermocline $\delta^{15}N$ maxima and ODZ depth was moderate ($r = -0.56$ to -0.70; $p < 0.001$), and the VIF values for these two predictors remained low (1.46–1.97), indicating minimal multicollinearity. At our study stations (Figure 3a), where the ODZ upper boundary lies below ~300 m, the $\delta^{15}N$ maxima at the core of the ODZs is higher than 10‰, while the subsurface nitrate $\delta^{15}N$ is only 6.3‰ (Figure 3b),

which is only slightly higher than the mean global average pycnocline nitrate $\delta^{15}N$ (Fripiat et al., 2021) and comparable to thermocline nitrate $\delta^{15}N$ outside modern ODZs in the eastern Pacific (Figures 3c–e). At these stations, based on FB-$\delta^{15}N$ values alone, one might not have inferred the presence of the underlying ODZs, suggesting that FB-$\delta^{15}N$ might be decoupled from the local, *in situ* water-column denitrification rates occurring immediately below. This decoupling between the thermocline ODZ $\delta^{15}N$ maxima and the subsurface $\delta^{15}N$ may be explained by the greater depth of ODZs, which impedes the diffusion of the high $\delta^{15}N$ signal from the thermocline into the subsurface, thereby reducing its influence on FB-$\delta^{15}N$ value. In addition, N_2 fixation in the surface waters, followed by subsequent remineralization in the subsurface, may further lower subsurface nitrate $\delta^{15}N$ (Wang et al., 2018). However, N_2 fixation rates appear to be limited in the eastern tropical Pacific (Knapp et al., 2016; Shao et al., 2023). Even if N_2 fixation were significant, its impact would be insufficient to override the elevated nitrate $\delta^{15}N$ produced by water-column denitrification, given the large isotope effect of water-column denitrification. Regardless of the mechanism, our compilation indicates that FB-$\delta^{15}N$ is less sensitive to local, *in situ* water column denitrification when the upper boundary of the ODZs is deeper than ~250 m, as observed at our new sites. Instead, FB-$\delta^{15}N$ at these stations appears to reflect broader regional denitrification. These findings suggest that variations in ODZ depths must be considered when interpreting FB-$\delta^{15}N$ records, as discussed below in Section 4.4.

4.2 Influence of ODZs on planktonic foraminifera habitat depths

Another impact of ODZs on FB-$\delta^{15}N$ arise from shifts in the habitat depths and species composition of foraminifera under low-oxygen conditions. While global variability in foraminifera habitat depths has been well-documented (*e.g.*, Ravelo and Fairbanks, 1992; Rebotim et al., 2017), few studies have specifically examined habitats under hypoxic (i.e., < 63 μmol/kg O_2) to suboxic conditions. The species analyzed in this study have been shown or hypothesized to tolerate hypoxic conditions (Kuroyanagi et al., 2013, 2019; Rippert et al., 2016). Davis et al. (2021) reported that suboxic-hypoxic conditions in an ETNP ODZ significantly affect the distribution and abundance of foraminifera. While some smaller specific species (size < 250 μm) exhibit adaptations that allow them to tolerate hypoxic conditions, the overall density and diversity of foraminifera decrease in the ODZs (Davis et al., 2021).

Globally, deep-dwelling species like *N. dutertrei*, *G. menardii*, and *G. tumida* typically inhabit depths below 100m (Ravelo and Fairbanks, 1992; Farmer et al., 2007). However, the eastern tropical Pacific ODZs exhibit hypoxic to suboxic conditions at such depths (Figure 3b). Notably, our data reveal that *N. dutertrei* and *G. menardii* are the most abundant species in these regions (Supplementary Figure S3). It is likely that these deep-dwelling species are forced to migrate upward, occupying shallower depths above the ODZs, where oxygen concentrations are more favorable for survival.

4.3 Inter-species variation in FB-$\delta^{15}N$ in ODZ regions

FB-$\delta^{15}N$ is also influenced by both the diet and symbiotic status of foraminifera (Bé and Hemleben, 1970; Anderson and Be, 1976; Bé et al., 1977; Caron and Bé, 1984; Spindler et al., 1984; Hemleben et al., 1989; Ren et al., 2012). The dietary habits of foraminifera vary among species and with depth in the water column. Surface-dwelling species prey on zooplankton and large phytoplankton using specialized spines for effective capture (Bé et al., 1977; Spindler et al., 1984) and are often symbiotic photosynthetic algae such as dinoflagellates. This symbiosis leads to lower $\delta^{15}N$ values because the symbionts efficiently recycle ammonium produced by their host, typically resulting in FB-$\delta^{15}N$ that are 0-1‰ lower than the subsurface nitrate $\delta^{15}N$ (Uhle et al., 1997; Ren et al., 2012; Smart et al., 2018). In contrast, deep-dwelling, symbiont-barren species exhibit higher $\delta^{15}N$ values (Ren et al., 2012; Smart et al., 2018), primarily due to the lack of symbiont-mediated nutrient recycling and the consumption of partially degraded organic matter with higher $\delta^{15}N$ (Ren et al., 2012).

Groundtruthing studies (Ren et al., 2012; Smart et al., 2018; Auderset et al., 2024) have documented inter-species differences in FB-$\delta^{15}N$ across the global ocean, driven by variations in diet and symbiotic associations as described in the previous paragraph. In oligotrophic waters with complete surface nitrate consumption, surface-dwelling, symbiont-bearing species show $\delta^{15}N$ similar to subsurface nitrate $\delta^{15}N$, whereas deep-dwelling, symbiont-barren species exhibit values 3-4‰ higher. For example, species such as *G. sacculifer* and *O. universa*, which host symbiotic dinoflagellates (Bé et al., 1977; Schiebel and Hemleben, 2017), show $\delta^{15}N$ values 0–1‰ lower than subsurface nitrate $\delta^{15}N$. Conversely, deep-dwelling, non-symbiotic species like *G. tumida* are 3-4‰ higher than subsurface nitrate $\delta^{15}N$. *N. dutertrei* and *G. menardii*, which host non-photosynthetic chrysophytes (Gastrich, 1987; Faber et al., 1988), show similar $\delta^{15}N$ as *G. tumida* (Ren et al., 2012). Our new results from an ODZ region are consistent with previous findings (Figure 4), with *G. tumida*, *N. dutertrei*, and *G. menardii* exhibiting $\delta^{15}N$ values that are 3-4‰ higher $\delta^{15}N$ than those of *G. sacculifer* and *O. universa*, which are similar to subsurface nitrate $\delta^{15}N$. This suggests that the presence of hypoxic conditions do not alter the inter-species differences in FB-$\delta^{15}N$.

4.4 Implications for reconstructing the history of ODZs

The findings from this study have important implications for using FB-$\delta^{15}N$ (and other $\delta^{15}N$ archives) as a proxy to reconstruct historical variations in ODZs. While previous studies have primarily used FB-$\delta^{15}N$ to indicate ODZ expansion or

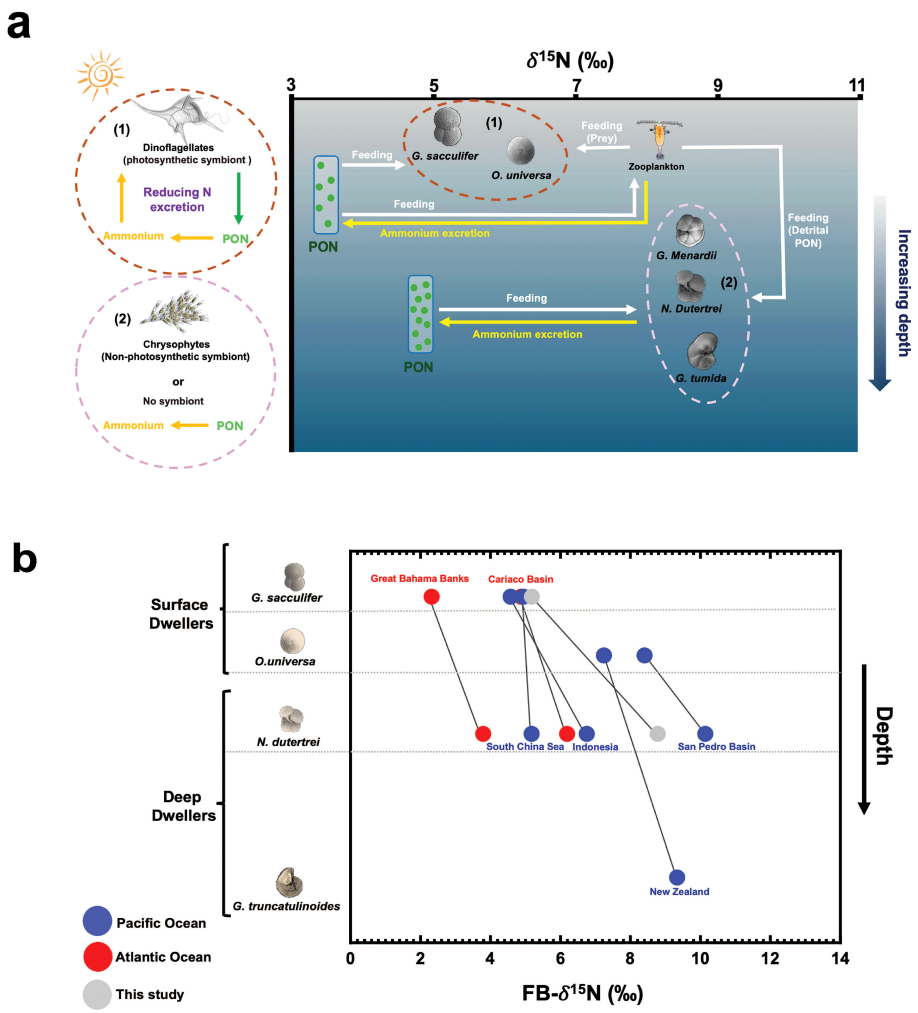

FIGURE 4
(a) Diagram illustrating difference in FB-δ^{15}N among planktonic foraminifera species within the ETNP ODZ, comparing surface-dwelling symbiont-bearing spinose species (dark red dashed circle, (1)) to deeper-dwelling symbiont-bearing non-spinose and non-symbiont-bearing non-spinose species (pink dashed circle, (2)). The x-axis represents the δ^{15}N values for all organisms in the diagram. Deeper in the water column, the particulate organic nitrogen (PON) consumed by foraminifera is higher in δ^{15}N, with the δ^{15}N of suspended PON increasing down the water column (Altabet, 1988). The overall concept of this diagram is adapted from Ren et al., 2012 and Smart et al., 2018. **(b)** Depth profile of FB-δ^{15}N for surface dwellers (i.e. *G. sacculifer* and *O. universa*) and deep dwellers (i.e. *N. dutertei*, and *G. truncatulinoides*) from previous studies (Ren et al., 2012; blue circles: Atlantic Ocean, red circles: Pacific Ocean) and from this study (grey circles).

contraction (Kast et al., 2019; Studer et al., 2021; Auderset et al., 2022; Wang et al., 2022; Hess et al., 2023; Moretti et al., 2024; Yao et al., 2024), our analyses reveal that ODZ depth also influences FB-δ^{15}N. Below, we propose two potential scenarios for this influence (Figures 5a–c).

In the first scenario, under a warmer climate, organic matter remineralization may occur at shallower depths due to the temperature dependence of respiration (Boscolo-Galazzo et al., 2021; Gerace et al., 2023; Kim et al., 2023). This shift could result in an upward displacement of the thermocline δ^{15}N maxima without increasing their absolute values (Figure 5b). Consequently, FB-δ^{15}N might increase even if water-column denitrification rates remain unchanged, although further research is needed to determine whether such shifts occurred during past warm periods.

In the second scenario, increased organic matter export driven by stronger upwelling (Gutiérrez-Cárdenas et al., 2024) or elevated thermocline nutrient content is expected to both intensify the ODZs and shift them upward (Figure 5c). In this case, enhanced denitrification would raise both the thermocline δ^{15}N maximum and increased nitrate loss (lower N*, Figure 5), and the upward shift would facilitate the transfer of the elevated δ^{15}N signal to the subsurface, thereby increasing subsurface nitrate δ^{15}N (and FB-δ^{15}N). Here, the FB-δ^{15}N increase would be consistent with higher water-column denitrification rates, albeit in a non-linear manner as the ODZ depth change also contributed to the increase of FB-δ^{15}N.

Considering these factors, variations in ODZ depth should be considered when using FB-δ^{15}N to reconstruct ODZ history. Given the spatial complexity of ODZs, integrating multiple cores spanning from the ODZ interiors to regions beyond their modern boundaries

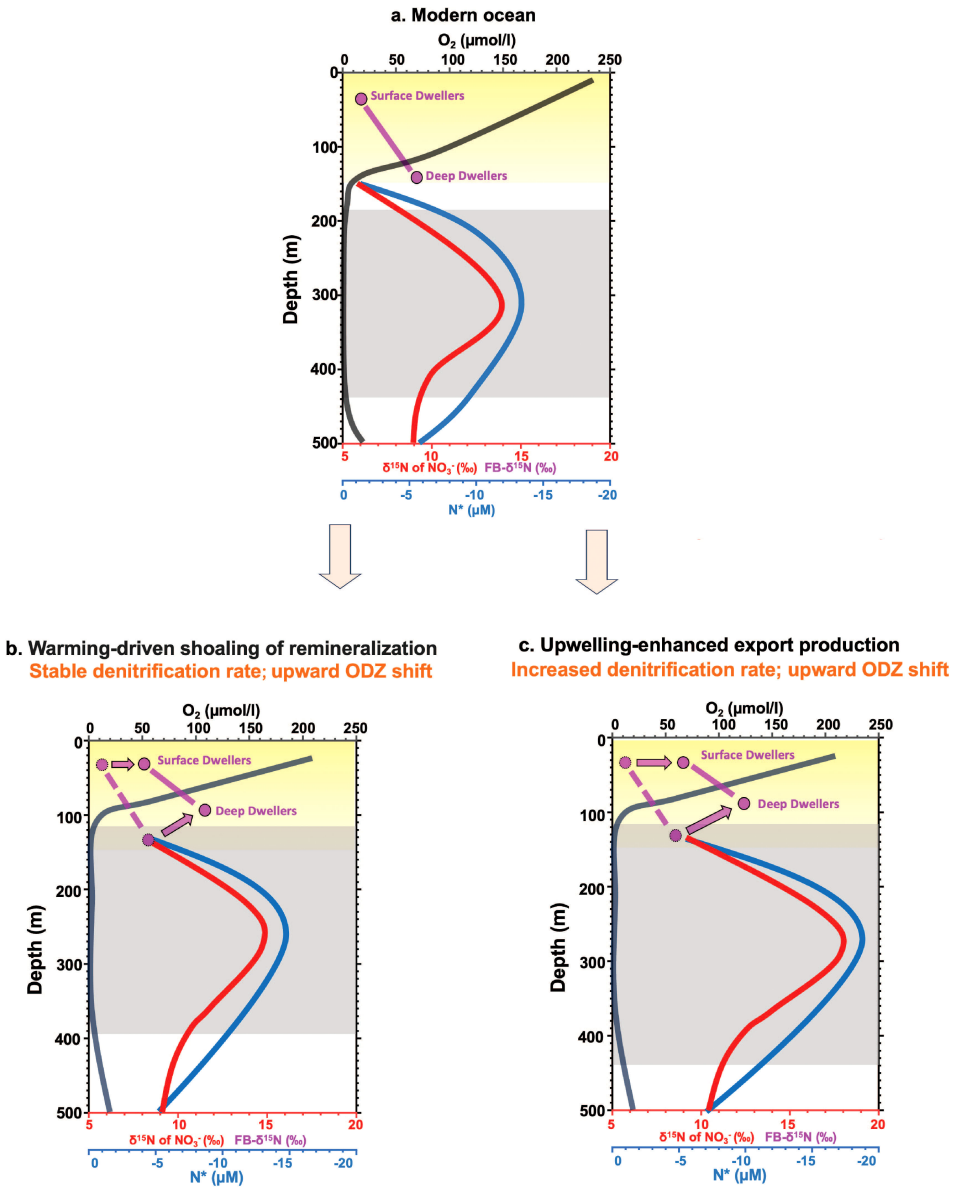

FIGURE 5
Schematic diagrams illustrating how ODZ depth changes may influence FB-$\delta^{15}N$ in both subsurface- and deep-dwelling foraminifera under two scenarios. **(a)** The top panel shows profiles representing the modern ocean, adapted after Casciotti et al. (2018), including depth profiles of nitrate and FB-$\delta^{15}N$ (‰), $N^*=[NO_3^-]-16[PO_4^{3-}]$ (μM), and oxygen concentration (μmol/L). Depth ranges of the ODZs (grey shaded area) and the euphotic zone (yellow shaded area) are indicated. The bottom two panels **(b, c)** show the hypothetical changes in these profiles and the corresponding shifts in ODZ depth under two scenarios: **(b)** warming-driven shoaling of remineralization and **(c)** upwelling-enhanced export production. In panels **(b, c)**, the FB-$\delta^{15}N$ offsets between subsurface and deep dwellers, shown in the modern ocean profiles, are indicated with dashed lines and arrows, highlighting the expected FB-$\delta^{15}N$ response under each scenario.

is critical for more robust reconstructions. As the elevated thermocline nitrate $\delta^{15}N$ signals within ODZs are laterally transported into adjacent regions outside modern ODZ boundaries, FB-$\delta^{15}N$ records from these peripheral areas primarily reflect ODZ expansions and contractions through time and broader regional changes in denitrification rates. In contrast, FB-$\delta^{15}N$ records from cores within modern ODZs provide complementary constraints on the intensity and vertical structure of the ODZs. Together, multiple FB-$\delta^{15}N$ records can provide a more comprehensive reconstruction of ODZ evolution.

5 Conclusion

In this study, we combined new and previously published $\delta^{15}N$ data from the eastern tropical Pacific ODZs to demonstrate that FB-$\delta^{15}N$ (and other $\delta^{15}N$ archives) from modern ODZ regions is a robust proxy for tracking past ocean deoxygenation, provided that changes in ODZ depths are considered in addition to water-column denitrification intensity. New $\delta^{15}N$ data from the eastern tropical North Pacific (5–8°N) suggest that, when ODZs are deep, subsurface nitrate $\delta^{15}N$ may not bear the signal of local denitrification

underneath. In these regions, FB-δ^{15}N may instead reflect broader regional denitrification rates, similar to locations outside today's ODZs. Consequently, interpreting FB-δ^{15}N records from ODZ regions requires careful consideration of potential shifts in ODZ depths. For instance, shallower organic matter remineralization under warmer climates—or deeper remineralization under colder conditions—could drive changes in FB-δ^{15}N without changes in water-column denitrification rates. In addition, low-oxygen conditions in ODZs may force deep-dwelling foraminiferal species to migrate upward, although current data do not indicate significant impacts on interspecies variations in FB-δ^{15}N. For a more robust reconstruction of ODZ history using FB-δ^{15}N, we recommend analyzing multiple sites along transects that span from within modern ODZs to adjacent regions beyond their current extent. Cores located outside present-day ODZs, yet still containing thermocline nitrate δ^{15}N signatures influenced by ODZs, are well suited for recording expansions and contractions of ODZs. In contrast, cores from within modern ODZs provide complementary insights into the ODZ's intensity and vertical structure. Combining these FB-δ^{15}N records allows for a more comprehensive understanding of ODZ evolution over time.

Data availability statement

The datasets presented in this study can be found in online repositories. The names of the repository/repositories and accession number(s) can be found in the article/Supplementary Material.

Author contributions

TK: Methodology, Data curation, Investigation, Writing – review & editing, Formal analysis, Writing – original draft, Visualization. TL: Writing – review & editing, Formal analysis, Writing – original draft, Methodology. KL: Methodology, Formal analysis, Writing – review & editing. RZ: Investigation, Methodology, Writing – review & editing. SD: Writing – review & editing, Methodology. XW: Project administration, Investigation, Writing – review & editing, Formal analysis, Methodology, Conceptualization, Writing – original draft, Funding acquisition.

Funding

The author(s) declare financial support was received for the research and/or publication of this article. This study was supported by the startup grant to XTW from Boston College. Publication fee was supported by the Boston College Open Access Publishing Fund.

Acknowledgments

We would like to thank the crew members and scientists for R/V Sally Ride SR2113.

In memoriam

Prof. Sijia Dong, a coauthor of this study, passed away while this manuscript was under review. An early-career scientist, her dedication, creativity, and collaborative spirit leave a lasting legacy in the field of the marine carbon cycle. She will be deeply missed by colleagues and the scientific community.

Conflict of interest

The authors declare that the research was conducted in the absence of any commercial or financial relationships that could be construed as a potential conflict of interest.

Generative AI statement

The author(s) declare that no Generative AI was used in the creation of this manuscript.

Publisher's note

Supplementary material

The Supplementary Material for this article can be found online at: https://www.frontiersin.org/articles/10.3389/fmars.2025.1600122/full#supplementary-material

References

Achacoso, S. C., Walag, A. M. P., and Saab, L. L. (2016). A rapid assessment of foliage spider fauna diversity in Sinaloc, El Salvador City, Philippines: a comparison between habitats receiving different degrees of disturbance. *Biodiversity* 17, 156–161. doi: 10.1080/14888386.2016.1258331

Altabet, M. A. (1988). Variations in nitrogen isotopic composition between sinking and suspended particles: implications for nitrogen cycling and particle transformation in the open ocean. *Deep Sea Res. Part A. Oceanographic Res. Papers* 35, 535–554. doi: 10.1016/0198-0149(88)90130-6

Anderson, O. R., and Be, A. W. H. (1976). The ultrastructure of a planktonic foraminifer, Globigerinoides sacculifer (Brady), and its symbiotic dinoflagellates. *J. Foraminiferal Res.* 6, 1–21. doi: 10.2113/gsjfr.6.1.1

Auderset, A., Moretti, S., Taphorn, B., Ebner, P.-R., Kast, E., Wang, X. T., et al. (2022). Enhanced ocean oxygenation during Cenozoic warm periods. *Nature* 609, 77–82. doi: 10.1038/s41586-022-05017-0

Auderset, A., Smart, S. M., Ryu, Y., Marconi, D., Ren, H. A., Heins, L., et al. (2024). Effects of photosymbiosis and related processes on planktic foraminifera-bound nitrogen isotopes in South Atlantic sediments. *EGUsphere* 22, 1–28. doi: 10.5194/egusphere-2024-2291

Bé, A. W., and Hemleben, C. (1970). Calcification in a living planktonic foraminifer, Globigerinoides sacculifer (BRADY). Available online at: https://www.researchgate.net/publication/230889356_Calcification_in_a_living_planktonic_foraminifer_Globigerinoides_sacculifer_BRADY (Accessed December 3, 2024).

Bé, A. W. H., Hemleben, C., Anderson, O. R., Spindler, M., Hacunda, J., and Tuntivate-Choy, S. (1977). Laboratory and field observations of living planktonic foraminifera. *Micropaleontology* 23, 155–179. doi: 10.2307/1485330

Bianchi, D., Dunne, J. P., Sarmiento, J. L., and Galbraith, E. D. (2012). Data-based estimates of suboxia, denitrification, and N2O production in the ocean and their sensitivities to dissolved O2. *Global Biogeochemical Cycles* 26. doi: 10.1029/2011GB004209

Boscolo-Galazzo, F., Crichton, K. A., Ridgwell, A., Mawbey, E. M., Wade, B. S., and Pearson, P. N. (2021). Temperature controls carbon cycling and biological evolution in the ocean twilight zone. *Science* 371, 1148–1152. doi: 10.1126/science.abb6643

Brady, H. B. (1877). II.—Supplementary note on the foraminifera of the chalk ()? of the new britain group. *Geological Magazine* 4, 534–536. doi: 10.1017/S0016756800150137

Brandes, J. A., Devol, A. H., Yoshinari, T., Jayakumar, D. A., and Naqvi, S. W. A. (1998). Isotopic composition of nitrate in the central Arabian Sea and eastern tropical North Pacific: A tracer for mixing and nitrogen cycles. *Limnology Oceanography* 43, 1680–1689. doi: 10.4319/lo.1998.43.7.1680

Breitburg, D., Levin, L. A., Oschlies, A., Grégoire, M., Chavez, F. P., Conley, D. J., et al. (2018). Declining oxygen in the global ocean and coastal waters. *Science* 359, eaam7240. doi: 10.1126/science.aam7240

Caron, D. A., and Bé, A. W. H. (1984). Predicted and observed feeding rates of the spinose planktonic foraminifer globigerinoides sacculifer. *Bull. Mar. Sci.* 35, 1–10.

Casciotti, K. L. (2016). Nitrogen and oxygen isotopic studies of the marine nitrogen cycle. *Annu. Rev. Mar. Sci.* 8, 379–407. doi: 10.1146/annurev-marine-010213-135052

Casciotti, K. L., Buchwald, C., and McIlvin, M. (2013). Implications of nitrate and nitrite isotopic measurements for the mechanisms of nitrogen cycling in the Peru oxygen deficient zone. *Deep Sea Res. Part I* 80, 78–93. doi: 10.1016/j.dsr.2013.05.017

Casciotti, K. L., Forbes, M., Vedamati, J., Peters, B. D., Martin, T. S., and Mordy, C. W. (2018). Nitrous oxide cycling in the Eastern Tropical South Pacific as inferred from isotopic and isotopomeric data. *Deep Sea Res. Part II* 156, 155–167. doi: 10.1016/j.dsr2.2018.07.014

Chavez, F. P., and Barber, R. T. (1987). An estimate of new production in the equatorial Pacific. *Deep Sea Res. Part A. Oceanographic Res. Papers* 34, 1229–1243. doi: 10.1016/0198-0149(87)90073-2

Cline, J. D., and Kaplan, I. R. (1975). Isotopic fractionation of dissolved nitrate during denitrification in the eastern tropical north pacific ocean. *Mar. Chem.* 3, 271–299. doi: 10.1016/0304-4203(75)90009-2

Czeschel, R., Stramma, L., Weller, R. A., and Fischer, T. (2015). Circulation, eddies, oxygen, and nutrient changes in the eastern tropical South Pacific Ocean. *Ocean Sci.* 11, 455–470. doi: 10.5194/os-11-455-2015

d'Orbigny, A. D. (1839). *Foraminifères [of Cuba]* (Bertrand).

Davis, C. V., Wishner, K., Renema, W., and Hull, P. M. (2021). Vertical distribution of planktic foraminifera through an oxygen minimum zone: how assemblages and test morphology reflect oxygen concentrations. *Biogeosciences* 18, 977–992. doi: 10.5194/bg-18-977-2021

DeVries, T., Deutsch, C., Primeau, F., Chang, B., and Devol, A. (2012). Global rates of water-column denitrification derived from nitrogen gas measurements. *Nat. Geosci* 5, 547–550. doi: 10.1038/ngeo1515

Faber, W. W., Anderson, O. R., Lindsey, J. L., and Caron, D. A. (1988). Algal-foraminiferal symbiosis in the planktonic foraminifer Globigerinella aequilateralia; I, Occurrence and stability of two mutually exclusive chrysophyte endosymbionts and their ultrastructure. *J. Foraminiferal Res.* 18, 334–343. doi: 10.2113/gsjfr.18.4.334

Farmer, E. C., Kaplan, A., de Menocal, P. B., and Lynch-Stieglitz, J. (2007). Corroborating ecological depth preferences of planktonic foraminifera in the tropical Atlantic with the stable oxygen isotope ratios of core top specimens. *Paleoceanography* 22. doi: 10.1029/2006PA001361

Fiedler, P. C., Philbrick, V., and Chavez, F. P. (1991). Oceanic upwelling and productivity in the eastern tropical Pacific. *Limnology Oceanography* 36, 1834–1850. doi: 10.4319/lo.1991.36.8.1834

Fiedler, P. C., and Talley, L. D. (2006). Hydrography of the eastern tropical Pacific: A review. *Prog. Oceanography* 69, 143–180. doi: 10.1016/j.pocean.2006.03.008

Fripiat, F., Martínez-García, A., Marconi, D., Fawcett, S. E., Kopf, S. H., Luu, V. H., et al. (2021). Nitrogen isotopic constraints on nutrient transport to the upper ocean. *Nat. Geosci.* 14, 855–861. doi: 10.1038/s41561-021-00836-8

Gastrich, M. D. (1987). Ultrastructure of a new intracellular symbiotic alga found within Planktonic Foraminifera. *J. Phycology* 23, 623–632. doi: 10.1111/j.1529-8817.1987.tb04215.x

Gerace, S. D., Fagan, A. J., Primeau, F. W., Moreno, A. R., Lethaby, P., Johnson, R. J., et al. (2023). Depth variance of organic matter respiration stoichiometry in the subtropical North Atlantic and the implications for the global oxygen cycle. *Global Biogeochemical Cycles* 37, e2023GB007814. doi: 10.1029/2023GB007814

Gruber, N. (2008). The marine nitrogen cycle: overview and challenges. *Carpenter* (San Diego: Academic Press), 1–50. doi: 10.1016/B978-0-12-372522-6.00001-3

Gutiérrez-Cárdenas, G. S., Morales-Acuña, E., Tenorio-Fernández, L., Gómez-Gutiérrez, J., Cervantes-Duarte, R., and Aguíñiga-García, S. (2024). El niño–Southern Oscillation diversity: effect on upwelling center intensity and its biological response. *J. Mar. Sci. Eng.* 12, 1061. doi: 10.3390/jmse12071061

Hemleben, C., Spindler, M., and Anderson, O. R. (1989). *Modern Planktonic Foraminifera.* (Springer Science & Business Media).

Hess, A. V., Auderset, A., Rosenthal, Y., Miller, K. G., Zhou, X., Sigman, D. M., et al. (2023). A well-oxygenated eastern tropical Pacific during the warm Miocene. *Nature* 619, 521–525. doi: 10.1038/s41586-023-06104-6

Hinkle, D. E., Wiersma, W., and Jurs, S. G. (2003). *Applied Statistics for the Behavioral Sciences.* (Houghton Mifflin).

Jobson, J. D. (1991). "Multiple linear regression," in *Applied Multivariate Data Analysis: Regression and Experimental Design*. Ed. J. D. Jobson (Springer, New York, NY), 219–398. doi: 10.1007/978-1-4612-0955-3_4

Kast, E. R., Stolper, D. A., Auderset, A., Higgins, J. A., Ren, H., Wang, X. T., et al. (2019). Nitrogen isotope evidence for expanded ocean suboxia in the early Cenozoic. *Science* 364, 386–389. doi: 10.1126/science.aau5784

Kim, H. H., Laufkötter, C., Lovato, T., Doney, S. C., and Ducklow, H. W. (2023). Projected 21st-century changes in marine heterotrophic bacteria under climate change. *Front. Microbiol.* 14. doi: 10.3389/fmicb.2023.1049579

Knapp, A. N., Casciotti, K. L., Berelson, W. M., Prokopenko, M. G., and Capone, D. G. (2016). Low rates of nitrogen fixation in eastern tropical South Pacific surface waters. *Proc. Natl. Acad. Sci.* 113, 4398–4403. doi: 10.1073/pnas.1515641113

Kuroyanagi, A., da Rocha, R. E., Bijma, J., Spero, H. J., Russell, A. D., Eggins, S. M., et al. (2013). Effect of dissolved oxygen concentration on planktonic foraminifera through laboratory culture experiments and implications for oceanic anoxic events. *Mar. Micropaleontology* 101, 28–32. doi: 10.1016/j.marmicro.2013.04.005

Kuroyanagi, A., Toyofuku, T., Nagai, Y., Kimoto, K., Nishi, H., Takashima, R., et al. (2019). Effect of euxinic conditions on planktic foraminifers: culture experiments and implications for past and future environments. *Paleoceanography Paleoclimatology* 34, 54–62. doi: 10.1029/2018PA003539

Kutner, M. H. (2005). *Applied Linear Statistical Models* (McGraw-Hill Irwin).

Kwiecinski, J. V., and Babbin, A. R. (2021). A high-resolution atlas of the Eastern tropical pacific oxygen deficient zones. *Global Biogeochemical Cycles* 35, e2021GB007001. doi: 10.1029/2021GB007001

Landry, K., and Wang, X. (2024). Average nitrate d15N values from the upper 1000 meters of the water column at four stations sampled in the Eastern Tropical North Pacific on R/V Sally Ride cruise SR2113 in December 2021. doi: 10.26008/1912/BCO-DMO.933292.1

Lee, C. W. M., Altabet, M., Mnich, A., and Zhang, L. (2025). Using δ15N of amino acids and nitrate to investigate particle production and transformation in the ocean: A case study from the Eastern Tropical North Pacific oxygen deficient zone. *Global Biogeochemical Cycles* 39, e2024GB008280. doi: 10.1029/2024GB008280

Liu, K.-K., and Kaplan, I. R. (1989). The eastern tropical Pacific as a source of 15N-enriched nitrate in seawater off southern California. *Limnology Oceanography* 34, 820–830. doi: 10.4319/lo.1989.34.5.0820

Luyten, J. R., Pedlosky, J., and Stommel, H. (1983). *The Ventilated Thermocline.* Available online at: https://journals.ametsoc.org/view/journals/phoc/13/2/1520-0485_1983_013_0292_tvt_2_0_co_2.xml (Accessed February 11, 2025).

Margolskee, A., Frenzel, H., Emerson, S., and Deutsch, C. (2019). Ventilation pathways for the north pacific oxygen deficient zone. *Global Biogeochemical Cycles* 33, 875–890. doi: 10.1029/2018GB006149

Martínez-García, A., Sigman, D. M., Ren, H., Anderson, R. F., Straub, M., Hodell, D. A., et al. (2014). Iron fertilization of the Subantarctic ocean during the last ice age. *Science* 343, 1347–1350. doi: 10.1126/science.1246848

Mehra, O. P., and Jackson, M. L. (1958). Iron oxide removal from soils and clays by a dithionite-citrate system buffered with sodium bicarbonate. *Clays Clay Miner.* 7, 317–327. doi: 10.1346/CCMN.1958.0070122

Moretti, S., Auderset, A., Deutsch, C., Schmitz, R., Gerber, L., Thomas, E., et al. (2024). Oxygen rise in the tropical upper ocean during the Paleocene-Eocene Thermal Maximum. *Science* 383, 727–731. doi: 10.1126/science.adh4893

O'brien, R. M. (2007). A caution regarding rules of thumb for variance inflation factors. *Qual Quant* 41, 673–690. doi: 10.1007/s11135-006-9018-6

Paulmier, A., and Ruiz-Pino, D. (2009). Oxygen minimum zones (OMZs) in the modern ocean. *Prog. Oceanography* 80, 113–128. doi: 10.1016/j.pocean.2008.08.001

Peters, B., Horak, R., Devol, A., Fuchsman, C., Forbes, M., Mordy, C. W., et al. (2018b). Estimating fixed nitrogen loss and associated isotope effects using concentration and isotope measurements of NO3–, NO2–, and N2 from the Eastern

Tropical South Pacific oxygen deficient zone. *Deep Sea Res. Part II: Topical Stud. Oceanography* 156, 121–136. doi: 10.1016/j.dsr2.2018.02.011

Peters, B. D., Lam, P. J., and Casciotti, K. L. (2018a). Nitrogen and oxygen isotope measurements of nitrate along the US GEOTRACES Eastern Pacific Zonal Transect (GP16) yield insights into nitrate supply, remineralization, and water mass transport. *Mar. Chem.* 201, 137–150. doi: 10.1016/j.marchem.2017.09.009

Rafter, P. A., and Sigman, D. M. (2016). Spatial distribution and temporal variation of nitrate nitrogen and oxygen isotopes in the upper equatorial Pacific Ocean. *Limnology Oceanography* 61, 14–31. doi: 10.1002/lno.10152

Rafter, P. A., Sigman, D. M., Charles, C. D., Kaiser, J., and Haug, G. H. (2012). Subsurface tropical Pacific nitrogen isotopic composition of nitrate: Biogeochemical signals and their transport. *Global Biogeochemical Cycles* 26. doi: 10.1029/2010GB003979

Ravelo, A. C., and Fairbanks, R. G. (1992). Oxygen isotopic composition of multiple species of planktonic foraminifera: recorders of the modern photic zone temperature gradient. *Paleoceanography* 7, 815–831. doi: 10.1029/92PA02092

Rebotim, A., Voelker, A. H. L., Jonkers, L., Waniek, J. J., Meggers, H., Schiebel, R., et al. (2017). Factors controlling the depth habitat of planktonic foraminifera in the subtropical eastern North Atlantic. *Biogeosciences* 14, 827–859. doi: 10.5194/bg-14-827-2017

Ren, H., Sigman, D. M., Meckler, A. N., Plessen, B., Robinson, R. S., Rosenthal, Y., et al. (2009). Foraminiferal isotope evidence of reduced nitrogen fixation in the ice age Atlantic Ocean. *Science* 323, 244–248. doi: 10.1126/science.1165787

Ren, H., Sigman, D. M., Thunell, R. C., and Prokopenko, M. G. (2012). Nitrogen isotopic composition of planktonic foraminifera from the modern ocean and recent sediments. *Limnology Oceanography* 57, 1011–1024. doi: 10.4319/lo.2012.57.4.1011

Rippert, N., Nürnberg, D., Raddatz, J., Maier, E., Hathorne, E., Bijma, J., et al. (2016). Constraining foraminiferal calcification depths in the western Pacific warm pool. *Mar. Micropaleontology* 128, 14–27. doi: 10.1016/j.marmicro.2016.08.004

Robinson, R. S., Smart, S. M., Cybulski, J. D., McMahon, K. W., Marcks, B., and Nowakowski, C. (2023). Insights from fossil-bound nitrogen isotopes in diatoms, foraminifera, and corals. *Annu. Rev. Mar. Sci.* 15, 407–430. doi: 10.1146/annurev-marine-032122-104001

Schiebel, R., and Hemleben, C. (2017). *Planktic Foraminifers in the Modern Ocean*. (Berlin, Heidelberg: Springer). doi: 10.1007/978-3-662-50297-6

Schiebel, R., Smart, S. M., Jentzen, A., Jonkers, L., Morard, R., Meilland, J., et al. (2018). Advances in planktonic foraminifer research: New perspectives for paleoceanography. *Rev. Micropaléontologie* 61, 113–138. doi: 10.1016/j.revmic.2018.10.001

Shao, Z., Xu, Y., Wang, H., Luo, W., Wang, L., Huang, Y., et al. (2023). Global oceanic diazotroph database version 2 and elevated estimate of global oceanic N_2 fixation. *Earth System Sci. Data* 15, 3673–3709. doi: 10.5194/essd-15-3673-2023

Sigman, D. M., Casciotti, K. L., Andreani, M., Barford, C., Galanter, M., and Böhlke, J. K. (2001). A bacterial method for the nitrogen isotopic analysis of nitrate in seawater and freshwater. *Anal. Chem.* 73, 4145–4153. doi: 10.1021/ac010088e

Sigman, D. M., Granger, J., DiFiore, P. J., Lehmann, M. M., Ho, R., Cane, G., et al. (2005). Coupled nitrogen and oxygen isotope measurements of nitrate along the eastern North Pacific margin. *Global Biogeochemical Cycles* 19, 2005GB002458. doi: 10.1029/2005GB002458

Smart, S. M., Ren, H., Fawcett, S. E., Schiebel, R., Conte, M., Rafter, P. A., et al. (2018). Ground-truthing the planktic foraminifer-bound nitrogen isotope paleo-proxy in the Sargasso Sea. *Geochimica Cosmochimica Acta* 235, 463–482. doi: 10.1016/j.gca.2018.05.023

Spindler, M., Hemleben, C., Salomons, J. B., and Smit, L. P. (1984). Feeding behavior of some planktonic foraminifers in laboratory cultures. *J. Foraminiferal Res.* 14, 237–249. doi: 10.2113/gsjfr.14.4.237

Studer, A. S., Mekik, F., Ren, H., Hain, M. P., Oleynik, S., Martínez-García, A., et al. (2021). Ice age-holocene similarity of foraminifera-bound nitrogen isotope ratios in the eastern equatorial pacific. *Paleoceanog Paleoclimatol* 36, e2020PA004063. doi: 10.1029/2020PA004063

Uhle, M. E., Macko, S. A., Spero, H. J., Engel, M. H., and Lea, D. W. (1997). Sources of carbon and nitrogen in modern planktonic foraminifera: the role of algal symbionts as determined by bulk and compound specific stable isotopic analyses. *Organic Geochemistry* 27, 103–113. doi: 10.1016/S0146-6380(97)00075-2

Voss, M., Dippner, J. W., and Montoya, J. P. (2001). Nitrogen isotope patterns in the oxygen-deficient waters of the Eastern Tropical North Pacific Ocean. *Deep Sea Res. Part I: Oceanographic Res. Papers* 48, 1905–1921. doi: 10.1016/S0967-0637(00)00110-2

Wang, X. T., Cohen, A. L., Luu, V., Ren, H., Su, Z., Haug, G. H., et al. (2018). Natural forcing of the North Atlantic nitrogen cycle in the Anthropocene. *Proc. Natl. Acad. Sci.* 115, 10606–10611. doi: 10.1073/pnas.1801049115

Wang, X. T., Wang, Y., Auderset, A., Sigman, D. M., Ren, H., Martínez-García, A., et al. (2022). Oceanic nutrient rise and the late Miocene inception of Pacific oxygen-deficient zones. *Proc. Natl. Acad. Sci.* 119, e2204986119. doi: 10.1073/pnas.2204986119

Weigand, M. A., Foriel, J., Barnett, B., Oleynik, S., and Sigman, D. M. (2016). Updates to instrumentation and protocols for isotopic analysis of nitrate by the denitrifier method. *Rapid Commun. Mass Spectrometry* 30, 1365–1383. doi: 10.1002/rcm.7570

Yao, W., Kong, T., Wang, X. T., Zhai, R., Zhang, R., and Liu, Y. (2024). Expanded subsurface ocean anoxia in the Atlantic during the Paleocene-Eocene Thermal Maximum. *Nat. Commun.* 15, 9053. doi: 10.1038/s41467-024-53423-x